Electronic Supplementary Material (ESI) for Nanoscale.

Supporting Information

The Making and Breaking of Perovskite Photochromism Through Doping

Xiuling Li,[a] *Wei Zheng,*[a] *Yuhai Zhang*[*,a]

[a] Institute for Advanced Interdisciplinary Research (iAIR), University of Jinan, Jinan 250022, Shandong, P. R. China

EXPERIMENTAL SECTION

Chemicals.

Cesium chloride (CsCl, 99.9%, Macklin), indium chloride ($InCl_3$, 99.9%, Rhawn), silver chloride (AgCl, 99.5%, Macklin), manganese chloride ($MnCl_2$, analytical pure, 99.0%, Macklin), Ethylenediaminetetraacetic acid disodium salt ($C_{10}H_{14}N_2O_8Na_2 \cdot 2H_2O$, analytical pure, Damao Chemical Reagent Factory) and hydrochloric acid (analytical pure, Yantai Far East Fine Chemical Co., Ltd., China.) All chemicals were used as received without further purification.

Synthesis of Perovskite Single Crystals by a Hydrothermal Method.

For Mn-doped $Cs_2AgInCl_6$ single crystals, 2 mmol CsCl, 1 mmol $InCl_3$, 1 mmol AgCl and variable amount (0.05, 0.1, 0.2, 0.4 mmol) of $MnCl_2$ were loaded into a 20-mL Teflon vessel before sealed in a stainless-steel cup. The cup was then kept at 180 °C for 12 hours and was allowed to slowly cool to 25 °C in 3200 minutes (3 °C/h). The cup was cooled naturally to room temperature. The as-prepared crystals were collected by decanting the solutions, and then washed with isopropanol before drying on a filter paper naturally. The Na/Mn co-doped crystals were prepared using an identical protocol as above, except for employing $C_{10}H_{14}N_2O_8Na_2 \cdot 2H_2O$ (0.2 mmol) as the sodium source.

X-ray Diffraction Measurements.

Powder X-ray diffraction (XRD) patterns were collected on grounded crystals using an X-ray diffractometer (Rigaku Ultima IV) coupled with Cu-Ka radiation (λ = 1.5406 Å). The scanning rate was set at 10 °/min with a step size of 0.02°.

Optical Photographs of Single Crystals

Optical photographs of crystals were taken by Canon 90D camera. The exposure time and ISO of optical photographs under daylight were 1/4 s and 400 respectively, and the exposure time and ISO under 365-nm and 254-nm ultraviolet lamp were 1/4 s and 6400.

Photochromic images of crystals were taken under white-LED lights. ISO and exposure time were set to 500 and 1/4.

Steady-state Photoluminescence Measurement.

The PL, PLE, 2D mapping and PL QY were measured using a FS5 spectrofluorometer (Edinburgh Instruments) equipped with an integrated sphere. PL and PLE tests were excited with a Xe lamp.

UV-vis Absorption Measurements.

Powder absorption diffuse reflectance measurements were performed in the range of 400-700 nm using an ultraviolet-visible spectrophotometer (EVOLUTION 201 Thermo Scientific Corporation).

Transient Photoluminescence Measurement.

The transient photoluminescence spectra of single crystals were measured with a time-resolved spectrometer (Delta-flex, Horiba Scientific). The crystals were excited with a 355-nm LED lamp with a temporal resolution ranging from microsecond to millisecond.

Table S1. ICP result of actual molar ratio of elements in $Cs_2Na_{0.4}AgInCl_6$: 20% Mn^{2+}.

Cs (%)	Na (%)	Ag (%)	In (%)	Mn (%)
141.75	46.94	0.42	100	0.12

Table S2. Interplanar spacing variation (Δd) of the (022) plane.

Nominal conc. (%)	Δd (%)
0% Mn	0
1% Mn	-0.14
2.5% Mn	0.38
5% Mn	0.63
7.5% Mn	0.89
10% Mn	0.52
20% Mn	0.62
40% Mn	0.63

The interplanar spacing (d) of the (022) plane could be calculated by Bragg equation:

$$d=\frac{n\lambda}{2sin\theta}$$

where λ was the x-ray wavelength (λ=0.15406), d was the spacing of the diffracting planes, n was an integer, the value of *n* could be considered to be 1 and θ was the angle between the incident rays and the diffracting planes, respectively.

The interplanar spacing variation (Δd) of the (022) plane could be calculated by the following equation:

$$\Delta d = \left(\frac{d_x - d_0}{d_0}\right) \times 100\%$$

where, d_x and d_0 was the d value when the nominal concentration of Mn^{2+} was x and 0 respectively.

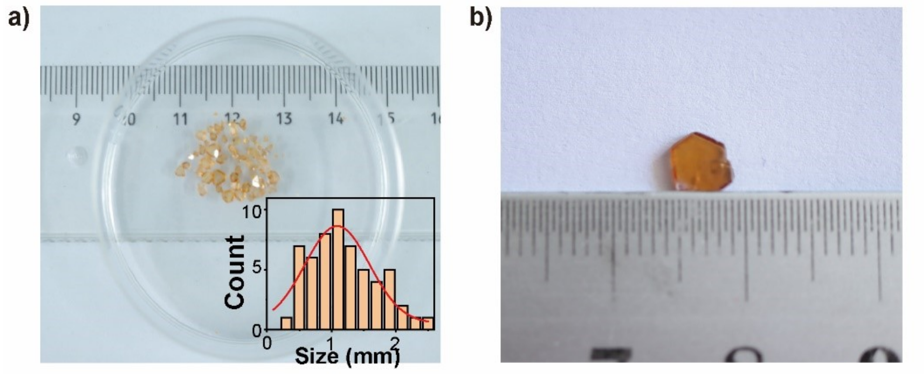

Figure S1. Photograph of $Cs_2AgInCl_6$: 5% Mn crystals. (a) The size of crystals fell in a range between 1-2 mm with cooling rate of 3 ^{o}C/h. (b) A 5-mm crystal was grown with a cooling rate of 1.5 ^{o}C/h.

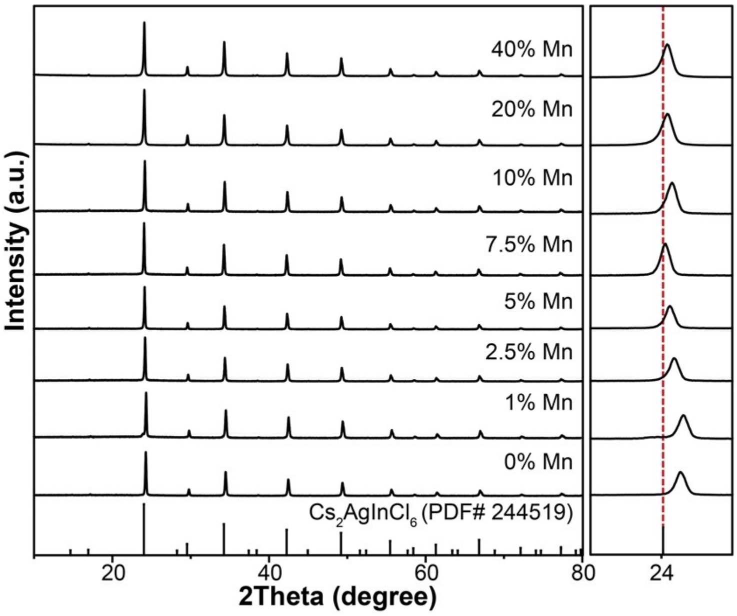

Figure S2. XRD pattern of $Cs_2AgInCl_6$: x% Mn crystals. The magnified (022) peak showed an irregular deviation with Mn ions doping, indicating a possible doping site of interstitial. Note that the 6-fold EPR signal suggested a high spin state of Mn2+， corresponding to a larger ionic radius of 0.83 Å. As shown in Figure S2, the (022) peak shifted to lower angle when increasing concentration from 1% to 7.5 %, indicating a lattice expansion. In this case, the lattice-site substitution of In3+ (0.8 Å) was possible based on the (022) peak shift. To further validate such conjecture, EDS measurement was conducted on 1% and 10% Mn-doped crystals, which suggested a low content in actual lattice (~ 1%). According to Vegard's law, the expected lattice expansion was only ~0.04%. However, the experimental data of interplanar spacing showed an expansion value of 0.5% (Figure 1b), which did not echo well with the conjecture of site substitution. Therefore, we proposed that Mn2+ took a possible doping site of interstitial.

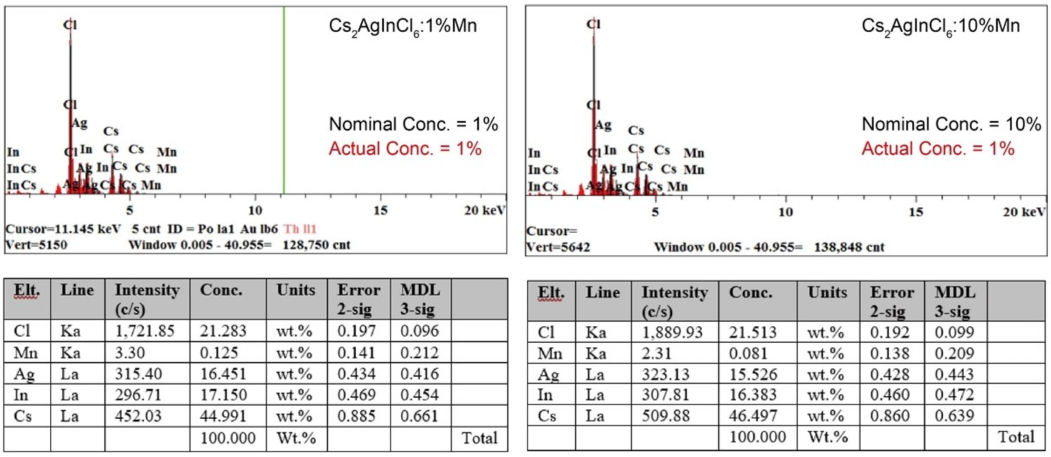

Elt.	Line	Intensity (c/s)	Conc.	Units	Error 2-sig	MDL 3-sig	
Cl	Ka	1,721.85	21.283	wt.%	0.197	0.096	
Mn	Ka	3.30	0.125	wt.%	0.141	0.212	
Ag	La	315.40	16.451	wt.%	0.434	0.416	
In	La	296.71	17.150	wt.%	0.469	0.454	
Cs	La	452.03	44.991	wt.%	0.885	0.661	
			100.000	Wt.%			Total

Elt.	Line	Intensity (c/s)	Conc.	Units	Error 2-sig	MDL 3-sig	
Cl	Ka	1,889.93	21.513	wt.%	0.192	0.099	
Mn	Ka	2.31	0.081	wt.%	0.138	0.209	
Ag	La	323.13	15.526	wt.%	0.428	0.443	
In	La	307.81	16.383	wt.%	0.460	0.472	
Cs	La	509.88	46.497	wt.%	0.860	0.639	
			100.000	Wt.%			Total

Figure S3. EDS measurements on Cs$_2$AgInCl$_6$: x% Mn crystals. The results exhibited an almost identical actual concentration of Mn ions, although the nominal concentration of Mn ions was largely different.

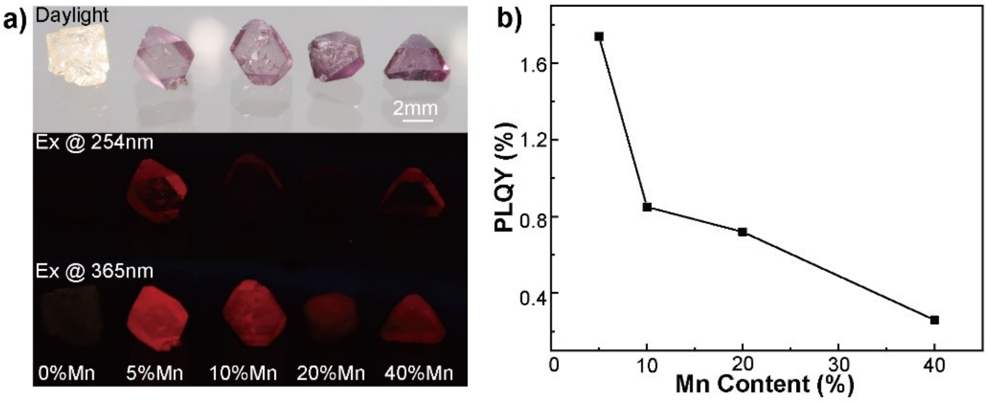

Figure S4. (a) Photographs of $Cs_2AgInCl_6$: x% Mn crystals under different light excitation. (b) PL QY of $Cs_2AgInCl_6$: x% Mn crystals under 350 nm excitation, indicating the optimized doping concentration of Mn^{2+} at 5%.

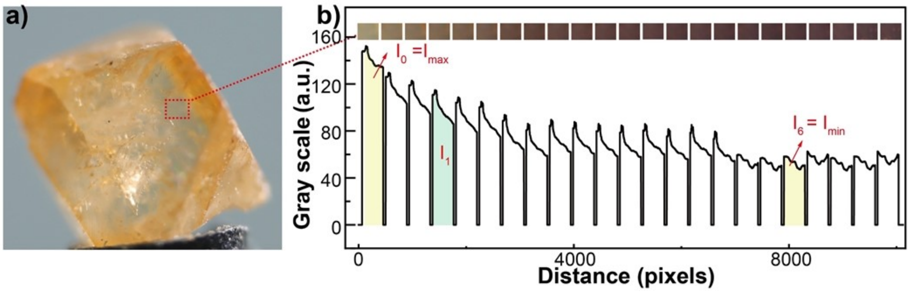

Figure S5. (a) Regions of interest (ROI) was taken from original image and (b) the corresponding gray scale of the whole ROI was extracted through Image J. In a typical calculation, the integrated area under gray-scale profile were denoted as $I_{max} = 55197$, $I_{min} = 20284$, and $I_1 = 39013$, respectively, as shown in Figure S4b. The I_B value at 1 minutes was calculated as follows:

$$I_B = \frac{I_t - I_{min}}{I_{max} - I_{min}} = \frac{39013 - 20284}{55197 - 20284} = 0.54$$

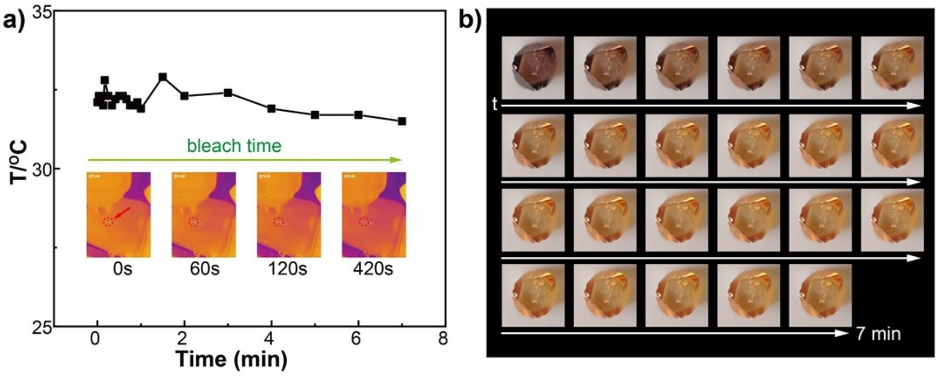

Figure S6. (a) The temperature of crystals upon 520-nm laser irradiation was monitored and plotted as a function of the irradiation time, indicating no significant change in temperature. (b) Photographs of Mn-doped crystals evolved over irradiation time.

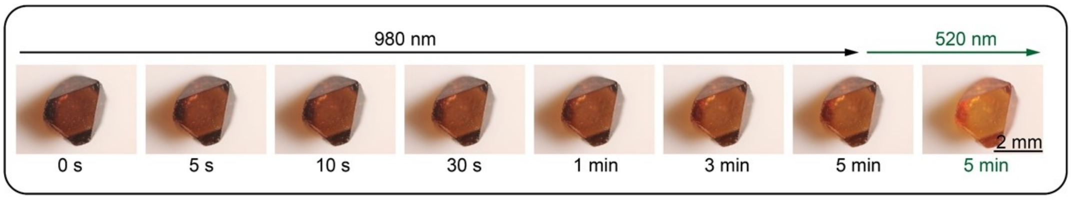

Figure S7. Photographs of colored $Cs_2AgInCl_6$: 5% Mn crystal upon 980-nm laser irradiation. The crystal hardly decolorated after irradiation with 980-nm laser (2.8 W/cm^2) for 5 min. However, the crystal was easily decolorated with a much weaker 520-nm laser (25 mW/cm2) for 5 min. The exposure time and ISO of optical photographs were 1/125 s and 2500, respectively.

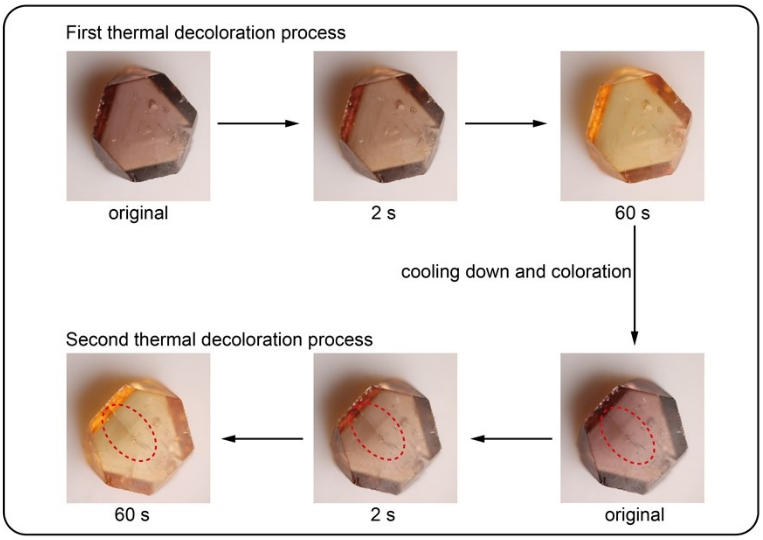

Figure S8. Photographs of $Cs_2AgInCl_6$: 5% Mn crystal under a coloration-decoloration cycle where heat was used for recovery at 200 ^{o}C. The dashed circle highlighted an obvious crack in the crystal from heat shock.

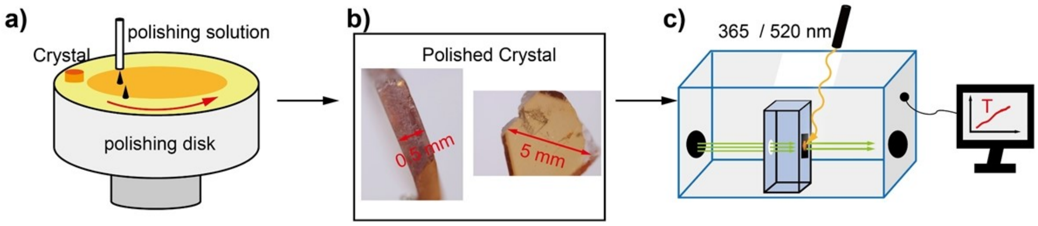

Figure S9. (a) Schematic showing a typical polishing process to obtain a flake-like crystal for transmittance measurement. (b) Photograph of a typical crystal flake. (c) Schematic showing the transmittance measurement of $Cs_2AgInCl_6$: 5% Mn crystals in real time.

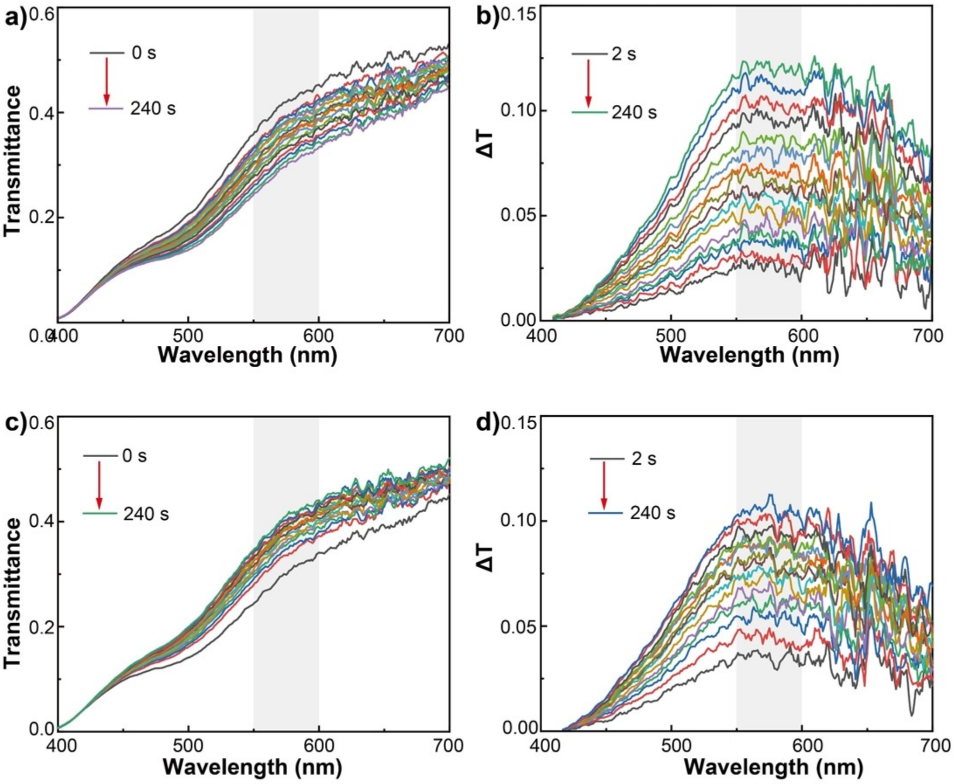

Figure S10. (a) The transmittance spectra of $Cs_2AgInCl_6$: 5% Mn single crystal under 365-nm light illumination evolved over time, showing a decrease in transmission intensity. (b) The transmittance difference spectra ($\Delta T = T_0 - T_t$) of $Cs_2AgInCl_6$: 5% Mn single crystal under 365-nm light illumination, showing a maximum transmittance difference at 550-600 nm. Note that the integrated area between 550 – 600 nm was used for calculation of T, and the ensuing ΔR_t in Figure 2d. (c) The transmittance spectra of $Cs_2AgInCl_6$: 5% Mn single crystal under 520-nm light illumination evolved over time, showing an increase in transmission intensity. (b) The transmittance difference spectra (ΔT) of $Cs_2AgInCl_6$: 5% Mn single crystal under 520-nm light illumination, showing a maximum transmittance difference at 550-600 nm.

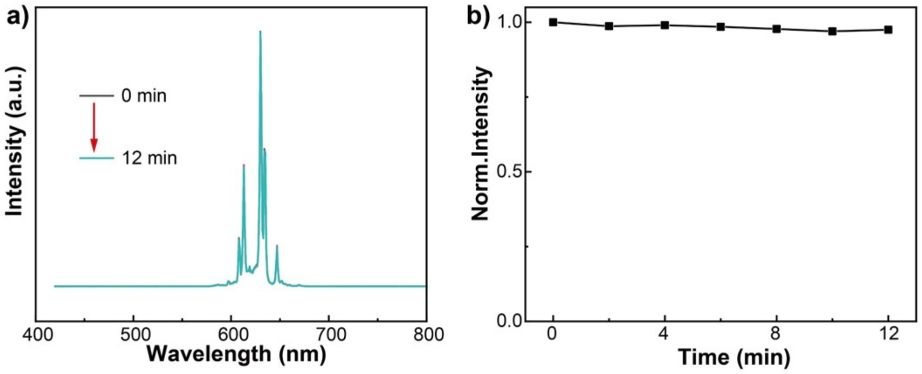

Figure S11. (a) PL spectra of a stable phosphor of KSF:Mn^{4+} were monitored for multiple times under 365-nm excitation, showing no significant change in intensity. (b) Integrated the area of PL profile against time showed a slight decay of 3%, which was ascribed to the excitation-lamp fluctuation.

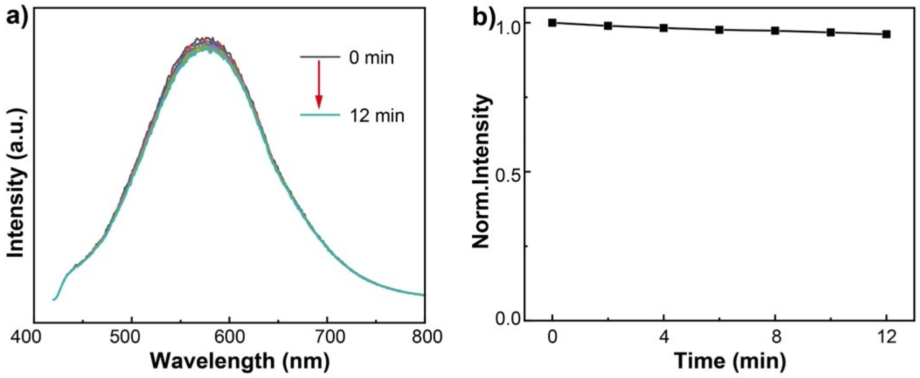

Figure S12. (a) PL spectra of $Cs_2Na_{0.4}Ag_{0.6}InCl_6$: 5% Mn crystals were monitored under 365-nm excitation. (b) Integrated the area under PL profile showed a 4% decay, similar to the stable phosphor of KSF:Mn^{4+}. Such robust stability was ascribed to the successful inhibition of photochromism by Na^+ doping.

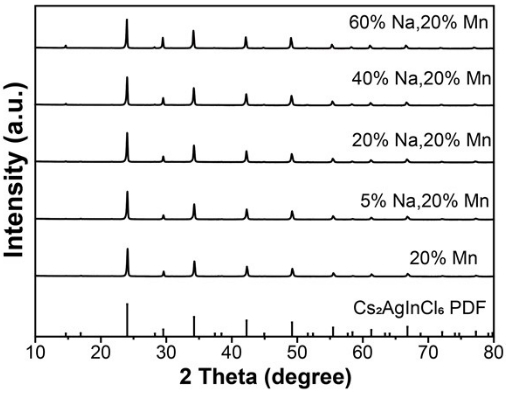

Figure S13. XRD patterns of $Cs_2Na_xAg_{1-x}InCl_6$: 20% Mn crystals. The crystal phase was well reserved even after a heavy doping of 60% Na^+.

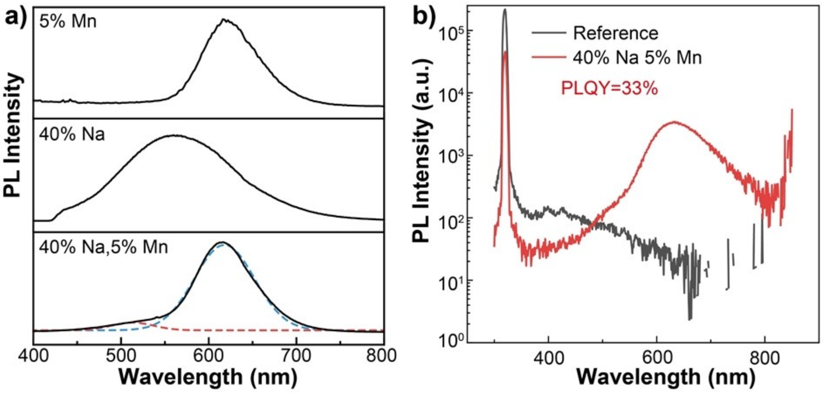

Figure S14. (a) Photoluminescence spectra of $Cs_2Na_xAg_{1-x}InCl_6$: y% Mn crystals. When only one ion was doped, the PL spectra was a single Gaussian peak. When Na-Mn was co-doped, it showed a dual-band emission. (a) PL QY measurements of $Cs_2Na_{0.4}Ag_{0.6}InCl_6$: 5% Mn crystals.

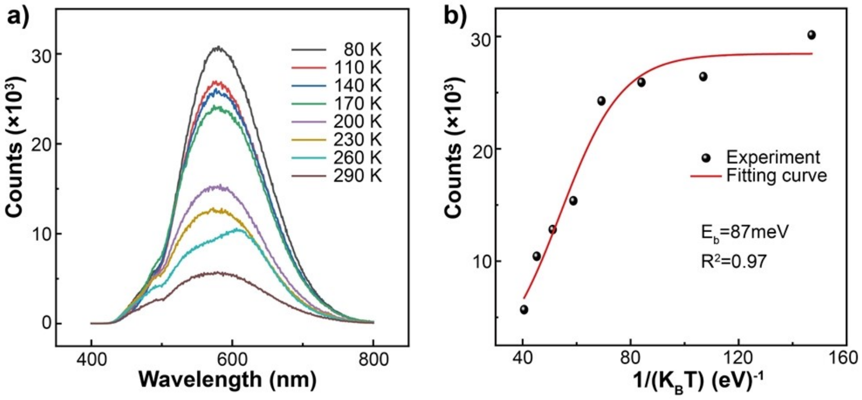

Figure S15. (a) Temperature-dependent PL spectra of $Cs_2Na_{0.4}Ag_{0.6}InCl_6$: 5% Mn crystals under 375-nm excitation. (b) PL intensity was fitted as a function of temperature according to the following equation:[1, 2]

$$\mathrm{I(T)} = \frac{I_0}{1 + Ae^{E_b/(k_B T)}}$$

Where, the I(T) and I_0 were the PL intensities at temperature T and 0 K, respectively. E_b was the exciton binding energy, and k_B was the Boltzmann constant, and the value was 8.5×10^{-5} eV/K.

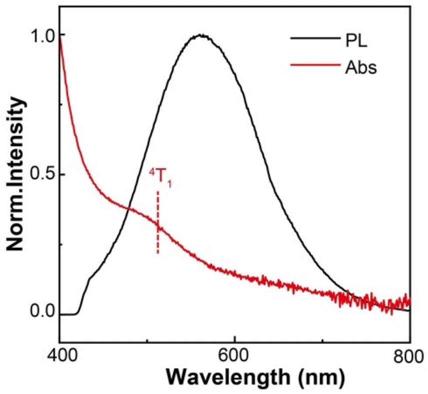

Figure S16. The absorption spectrum of $Cs_2AgInCl_6$: 5% Mn crystal showed an overlap with the STE emission from $Cs_2Na_{0.4}Ag_{0.6}InCl_6$ crystals, indicating a high possibility for the formation of a donor-acceptor (STE-Mn^{2+}) pair.

REFERENCE

(1) Chen, D.; Wan, Z.; Chen, X.; Yuan, Y.; Zhong, J. Large-scale room-temperature synthesis and optical properties of perovskite-related Cs_4PbBr_6 fluorophores. *Journal of Materials Chemistry C* **2016,** *4* (45), 10646.

(2) Liu, N.; Sun, R.; Wang, L.; Ji, Y.; Li, N.; Cao, B.; Zhang, Y. Unexpected red emission from Cs_4PbI_6 nanocrystals. *Journal of Materials Chemistry A* **2020,** *8* (12), 5952.